SimBuild 2024

Eleventh National Conference of IBPSA-USA
Denver, Colorado
May 21 – 23, 2024

Thermal comfort evaluation during demand response using Computational Fluid Dynamics (CFD)

Abstract

This study reevaluates HVAC systems in demand response initiatives, emphasizing end-user thermal comfort, a typically neglected aspect. Using Computational Fluid Dynamics, it assesses thermal comfort in a DOE reference small office, comparing mixing and displacement ventilation strategies under varying internal loads. Key metrics include Predicted Mean Votes, draft risk, and vertical temperature differences during response and recovery periods. Findings reveal displacement ventilation ensures faster temperature adjustments and potential energy savings, especially at higher internal loads. However, it's more sensitive to supply air temperature changes, affecting local thermal comfort. This underscores the importance of considering local thermal comfort.

Introduction

Demand response is defined as “changes in electric usage by end-use customers from their normal consumption pattern” (Albadi et al. 2008). Because heating, ventilating, and air-conditioning (HVAC) systems account for about 40% of buildings’ energy consumption (González-Torres et al. 2022) and provide flexible, repeatable, and predictable controllability (Yin et al. 2016, Shan et al. 2016), they have been a main target of demand response. As a typical demand response strategy for HVAC systems, global temperature adjustment increases cooling setpoint temperature for an entire facility during a response period in response to a grid signal (i.e., incentive-based) or electricity price (i.e., price-based) (Motegi et al.2007, Albadi et al. 2007, Wang et al. 2019). Following the response period, a recovery period is when the setpoint temperature returns to normal condition.

Most previous studies in the literature primarily focused on optimizing demand reduction and very little attention has been placed on thermal comfort. As illustrated in Table 1, numerous studies incorporate thermal comfort into their optimization frameworks, with a focus on maximizing demand reduction and introducing innovative strategies. However, these studies often treat thermal comfort merely as a constraint or a parameter to be optimized, rather than as a primary objective. Moreover, in these studies, simulation tools such as EnergyPlus and TRNSYS have been widely used (see Table 1). However, the aforementioned simulation tools assume a well-mixed room condition at a quasi-steady state, thereby neglecting spatial distributions of air temperature or velocity. Additionally, the tools do not offer detailed modelling of ventilation strategies (e.g., mixing and displacement) that can greatly influence occupants’ thermal comfort (Ahn et al. 2018). Because a steady-state thermal environment provides only well-mixed indoor air temperature and relative humidity, most studies relied on PMV or PPD as an indicator for thermal comfort assessments. However, a temperature ramp rate—a change in temperature over a time interval (Hamm et al. 2018)—needs to be assessed along with PMV as it can affect occupants’ thermal sensation and HVAC energy consumption (Wu et al. 2020).

Moreover, while the whole-body sensation (e.g., PMV) has been widely employed as a thermal comfort indicator, as shown in Table 1, local thermal comfort has not been considered. Arens et al. (2006) indicate that even in a uniform environment, body’s skin temperature and local comfort can vary. Similarly, the ASHRAE Standard 55 defines the local thermal discomfort as thermal discomfort caused by locally specific conditions such as a vertical air temperature difference between head and ankle and draft at ankle region (ASHRAE, 2020).

The objective of this study is to assess occupants’ thermal comfort under unsteady conditions during global temperature adjustments, using Computational Fluid Dynamics (CFD) simulations. We examined primarily two time periods: response and recovery periods. The former is when cooling setpoint temperature increases by a predefined magnitude and the latter is when it returns to the normal condition. To illustrate various possible cases, we considered two ventilation strategies (i.e., mixing and displacement) and three levels of internal load intensity (i.e., low, medium, and high). Occupants' adoptivity to indoor temperature varies over time (Aghniaey et al. 2018), requiring unsteady state simulation.

Methods

Description of a room geometry

Utilizing the advanced CFD software Star-CCM+, a simulation of a small office accommodating eight occupants has been developed. The 15 m × 10 m × 3 m space was based on the Department of Energy (DOE) reference building of small office core zone to emulate the typical small office environment. Figure 1 delineates the comprehensive geometry with features such as the supply diffusers for both mixing and displacement ventilation, exhausts, lighting fixtures, and desks, which supplant the electronic processes indicated in Appendix A's Reference Building Internal Load. Adhering to the DOE's stipulated occupant density of 18.6 m^2/person, eight sedentary occupants facing the front aligned with 2 rows with desks in front of each occupant. The supply diffusers for mixing and displacement ventilation are separated. The mixing ventilation system features four 0.2 m x 0.2 m units, each with a central blocked square, positioned at the ceiling. In contrast, the displacement ventilation employs six 0.5 m × 0.5 m sidewall diffusers at the floor level. Both ventilation techniques utilize shared exhaust systems. Specifically, the diffusers for displacement, placed at the floor level, release air vertically, while those designated for mixing, anchored at the ceiling, direct air in four distinct directions, each at a 30-degree angle from the ceiling.

For boundary conditions, as shown in Table 2, both mixing and displacement ventilation diffusers supply the same volume of air as a mass flow inlet, with the quantity dependent on the internal load; however, they have different supply air temperatures. The supply air temperatures for mixing ventilation and displacement ventilation are 15°C and 19°C, respectively. These temperatures were determined using the energy balance equation to achieve exhaust air temperatures of 23 °C for mixing ventilation and 27°C for displacement ventilation. The elevated supply air temperature for displacement ventilation is attributed to two factors: (1) displacement ventilation typically maintains a higher supply air temperature than mixing ventilation to reduce draught at the occupants' ankles, and (2) the supply diffusers are situated at the floor level, resulting in a comparable volume-averaged temperature in the ASHRAE breathing zone (0.075 m above ground, 0.6 m away from the sidewalls, and 1.8 m in height) to that of mixing ventilation, ranging between 21°C and 23°C. Each occupant generates 85 Watts of heat, with 40 Watts from convective heat from their body and 45 Watts of radiative heat uniformly distributed to the floor, sidewalls, and ceilings (Sørensen et al. 2003). While the heat output from the occupants remained constant, the heat loads from the desks and lights, as well as the supply

Table 1.Summary of demand response literature considered thermal comfort

Author	Year	Main objective		Thermal comfort indicator	Building type	Simulation tool
		Demand reduction	Thermal comfort			
Cui et al.	2015	✓	✓	Indoor air temperature	Office	TRNSYS
Xue et al.	2015	✓	✓	Indoor air temperature	Office	TRNSYS
Yoon et al.	2016	✓	✓	Indoor air temperature	Residential	EnergyPlus
Li et al.	2016	✓	✓	PMV	Office	• TRNSYS • EnergyPlus
Li and Malkawi	2016	✓	✓	PMV	Office	• EnergyPlus • GenOpt
Korkas et al.	2016	✓	✓	• PMV • PPD	• Commercial • Industrial • residential	EnergyPlus

airflow rate, were varied to align with the corresponding heat load intensity. This was done to investigate the effects of different levels of heat load on thermal comfort. Table 3 presents the various case scenarios examined.

Quality assurance for CFD simulation

To assure quality of the CFD model, verification of the mesh was executed via the computation of the grid convergence index (GCI), while the verification of the physics was conducted through assessments of mass and energy balances. In the context of the mass balance, as derived from Eq.(1), the CFD software tool, Star-CCM+, yielded a differential based upon the difference of supply and exhaust within the simulation domain, resulting in a value within < 0.001%. Pertaining to the energy balance, the exhaust air temperature, as derived from Eq. (2), was compared to the simulated air temperature on the exhaust's surface.

$$(\dot{m})_{in} = (\dot{m})_{out} \qquad (1)$$

Where $\dot{m}$ is mass flow rate in kg/s

$$Q = \rho \times \mathrm{V} \times C_p \times \left(\mathrm{T}_{Exhaust} - \mathrm{T}_{Supply}\right) \qquad (2)$$

Where Q is internal heat load in Watt, ρ is density of air in kg/m^3, V is volumetric flow rate of air in m^3/s, C_p is specific heat of air in kJ/(kg·K), $\mathrm{T}_{Exhaust}$ is temperature of air at exhaust in K, and T_{Supply} is temperature of air at supply in K.

In the realm of mesh verification, the Grid Convergence Index (GCI) method was used for estimating discretization errors (Celik et al. 2008). An excessively fine mesh can culminate in elevated computational expenditures, both in terms of time and resources.

Conversely, an overly coarse mesh is likely to yield results that lack precision. Consequently, the GCI method serves as an invaluable optimization tool, facilitating the identification of an optimal mesh count that balances computational efficiency with result accuracy.

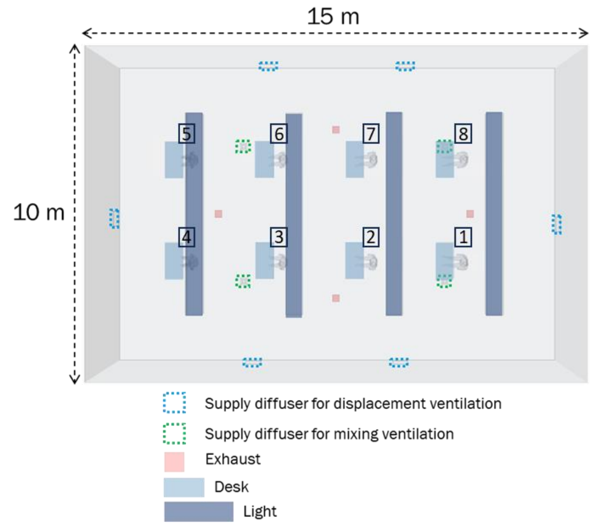

Figure 1 Top view of the simulation geometry with indications of supply diffusers, exhaust, desk, light, and occupant number.

$$GCI_{fine}^{21} = \frac{1.25 \times e_a^{21}}{r_{21}^{p} - 1} \qquad (3)$$

Where e_a^{21} is approximate relative error of parameter interested, r is grid refinement factor, and p is apparent order of convergence.

Three distinct mesh resolutions—grid 1, 2, and 3—are deployed, as shown in Figure 2, and the parameter of interest is the steady-state velocity simulated at a height of 0.2 m above an occupant's head.

The Grid Convergence Index (GCI) for these different resolutions is presented in Table 3. Correspondingly, Figure 3 illustrates the velocity profiles above an occupant's head, providing a comparative analysis across the three mesh resolutions. Upon rigorous evaluation via the GCI methodology and taking into account factors of computational time and resource, grid 2 is examined as the optimal choice for the current study.

Table 2 Summary of examined case scenarios

Ventilation strategy	Supply air temperature [℃]		Internal load intensity: level, value [W/m^2]	Supply air flow rate [L/s]
	Response period	Recovery period		
Mixing	17	15	Low, 26	375
			Medium, 45.7	665
			High, 67	801
Displacement	21	19	Low, 26	375
			Medium, 45.7	665
			High, 67	801

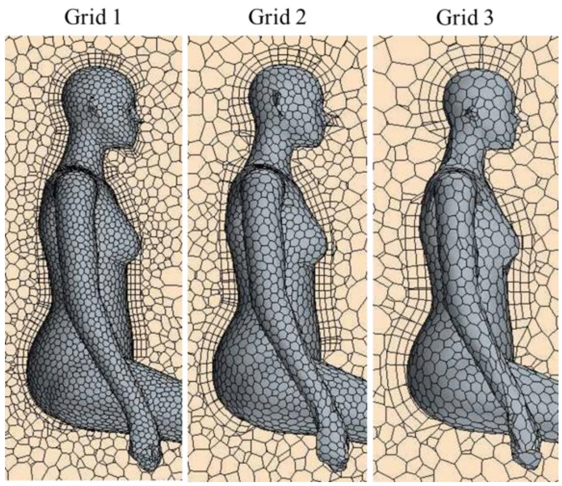

Figure 2 Three cross-sectional views of an occupant, each corresponding to a different grid layout.

Table 3 Grid convergence index (GCI) for the model

	Grid 1 (fine)	Grid 2 (medium, examine)	Grid 3 (coarse)
Number of cells	870,602	384,883	183,574
Grid refinement ratio	1.31	1.28	-
Air velocity at 0.2m above an occupant's head (m/s)	0.085	0.084	0.091
GCI (%)	0.3	1.5	-

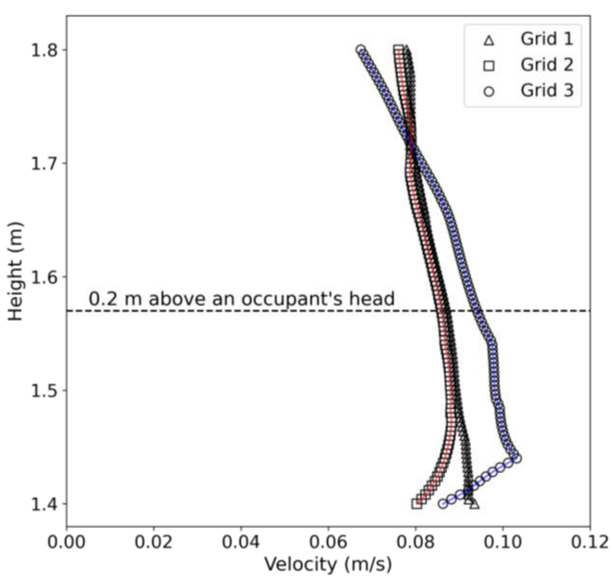

Figure 3 Velocity above an occupant's head comparing three different grids.

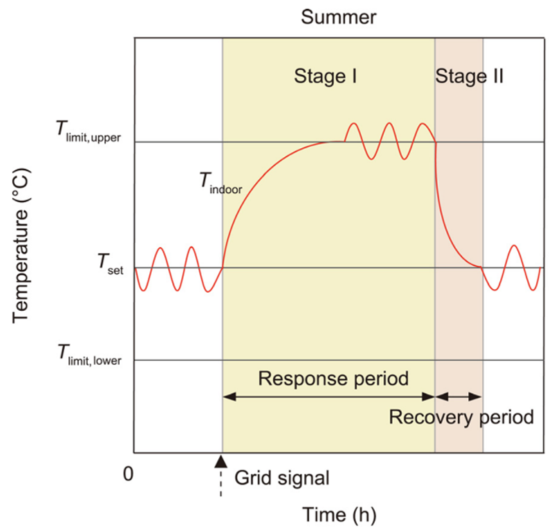

Figure 4. Illustration of global temperature adjustment reproduced from (Luo et al. 2022).

Description of global temperature adjustment

Figure 4 illustrates global temperature adjustment that raises a cooling setpoint temperature for entire zones in a building to reduce the peak electric demand (Yin et al. 2019). In this study, supply air temperature was increased by 2℃ from a normal temperature during 2 hours of a response period and returned to the normal temperature afterward (i.e., recovery period). A normal supply air temperature was maintained 4℃ higher for displacement ventilation (19℃) than mixing ventilation (15℃) to avoid local discomfort at an ankle level (Ahn et al. 2018, Wu et al. 2017).

Evaluation of occupants' thermal comfort

During response and recovery periods for each of the six examined scenarios, thermal comfort was assessed using three criteria: a time constant, predicted mean votes (PMVs), and draft risk. The time constant is often used in lumped or resistance-capacitance (RC) models and indicates the time required for a system to reach 63.2% of the difference between the start value and final value after a step change (Ning et al. 2015). In this study, the time required for the ASHRAE breathing zone to reach 63.2% of the maximum temperature difference (i.e., 2℃) was considered as the time constant. Because the time constant can determine temperature ramp rate, it can also be an indirect indicator of thermal comfort and HVAC energy consumption.

To understand the localized impacts of temperature ramp rate on individual occupants' thermal sensation, our study has established three distinct sampling volumes at ankle, chest, and head levels (see Figure 5).

According to the ASHRAE standard 55, the ankle and head levels were located at 0.1 m and 1.1 m above the floor, respectively, for seated individuals. From each sampling volume, the averaged air temperature and velocity in each scenario were monitored to assess the thermal comfort experienced by each occupant.

For eight occupants, we assessed unsteady- and steady-state PMVs. As unsteady-state PMVs, PMVs only until the time constant were considered. Unsteady-state PMVs could capture how occupants' thermal comfort varies during an early phase of a response or recovery period. On the other hand, steady-state PMVs are PMVs estimated from the one time constant to the end of a response or recovery period (see Figure 6). A PMV of the *n-th* occupant at the *i-th* time step (in this study, 200 min) was estimated using Eq. (4) (Fanger et al. 1972).

$$PMV_{n,i} = (0.303e^{-0.036M} + 0.028) \times \{(M-W) - 3.05 \times 10^{-3} \times [5733 - 6.99(M-W) - P_a] - 0.42 \times [(M-W) - 58.15] - 1.7 \times 10^{-5} \times M(5867 - P_a) - 0.0014 \times M \times (34 - t_a) - 3.96 \times 10^{-8} \times f_{cl} \times [(t_{cl}+273)^4 - (\bar{t}_r + 273)^4] - f_{cl} \times h_c \times (t_{cl} - t_a)\} \quad (4)$$

$$f_{cl} = \begin{cases} 1.00 + 1.290 \times I_{cl} \;\; for\; I_{cl} \leq 0.078\,\frac{m^2K}{W} \\ 1.05 + 0.645 \times I_{cl} \;\; for\; I_{cl} > 0.078\,\frac{m^2K}{W} \end{cases} \quad (5)$$

$$h_c = \begin{cases} 2.38 \times (t_{cl} - t_a)^{0.25} \\ for\; 2.38 \times (|t_{cl} - t_a|)^{0.25} > 12.1\sqrt{V_{ar}} \\ 12.1\sqrt{V_{ar}} \\ for\; 2.38 \times (|t_{cl} - t_a|)^{0.25} < 12.1\sqrt{V_{ar}} \end{cases} \quad (6)$$

$$t_{cl} = 35.7 - 0.028 \times (M - W) - I_{cl}\{3.96 \times 10^{-8} \times f_{cl} \times [(t_{cl}+273)^4 - (\bar{t}_r + 273)^4] - f_{cl} \times h_c \times (t_{cl} - t_a)\} \quad (7)$$

Where

M: Metabolic rate in $\frac{W}{m^2}$

W: Effective mechanical power in $\frac{W}{m^2}$

I_{cl}: Thermal resistance of clothing in $\frac{m^2\,°C}{W}$

f_{cl}: Ratio of surface area of the body with clothes to the surface area of the body without clothes

t_a: Air temperature in °C

$\bar{t}_r$: Mean radiant temperature in °C

V_{ar}: Relative air velocity in m/s

P_a: Water vapor partial pressure in Pa

h_c: Convective heat transfer coefficient in $\frac{W}{m^2\,°C}$

t_{cl}: Clothing surface temperature in °C

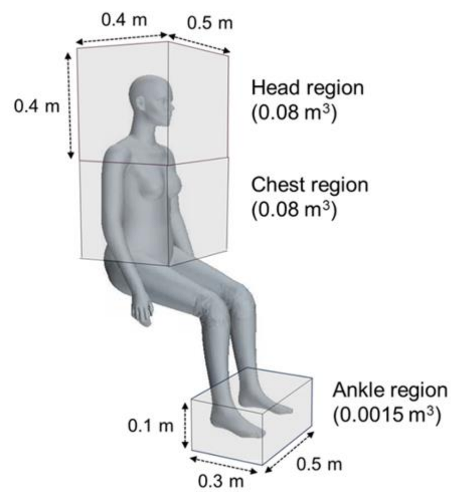

Figure 5 sampling volume at ankle, chest, and head levels

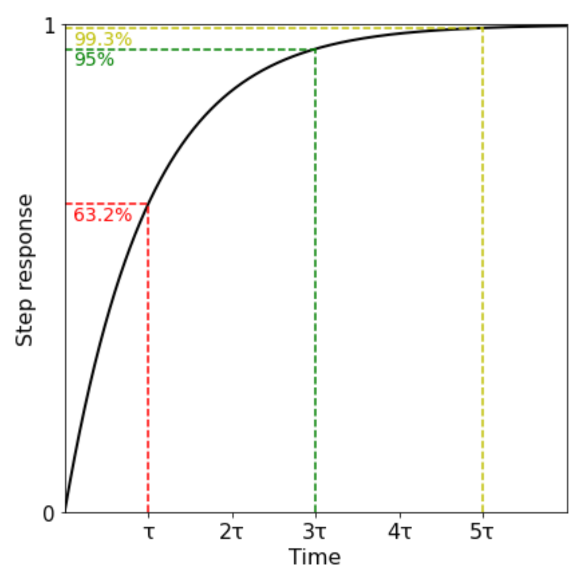

Figure 6 First order system step response plot.

Additionally, Eq. (7) (Fanger et al. 1988) is employed to estimate draft risks at ankle, chest, and head levels for each occupant, aiming to evaluate the thermal discomfort engendered by cool air movement. Draft risk is particularly pronounced in displacement ventilation systems, where air is supplied directly at ankle level, an area often exposed and sensitive to drafts. Sensitivity to draft is notably elevated in regions where the skin is not clothed, such as the head and leg areas, making it a critical concern during the cooling season (Cheng et al. 2015). Conversely, while less direct, mixing ventilation could also present overall draft risk due to elevated air velocities emanating from overhead diffusers (Shan et al. 2016). Therefore, this study comprehensively explores draft risks at different levels to understand the implications for thermal comfort under both ventilation strategies.

$$draft_{n,i,l} = \left(34 - t_{n,i,l}\right) \times \left(v_{n,i,l} - 0.05\right)^{0.62} \times \left(0.37 v_{n,i,l} Tu + 3.14\right) \tag{7}$$

where $draft_{n,i,l}$ indicates draft risk at a height level l (e.g., ankle, chest, and head) of the *n-th* occupant at the *i-th* time step; $t_{n,i,l}$ and $v_{n,i,l}$ indicate mean air temperature and velocity, respectively, within a sampling volume at the corresponding height level for that occupant and Tu indicate turbulence intensity.

Results and discussion

One time constant

Figure 7 shows that regardless of the internal load intensity displacement ventilation yields a 31-54% shorter time constant for the response period than mixing ventilation. A similar pattern is found for the recovery period. These observations can primarily be attributed to the characteristic of displacement ventilation systems, wherein floor-level diffusers directly channel air into the ASHRAE breathing zone (Ahn et al. 2018). Difference in time constants of two distribution systems becomes more pronounced with increasing internal load intensities.

Steady-state PMVs

Figures 8 and 9 present the PMV of the eight occupants over 200 minutes including the response and recovery periods. The Low internal load for both ventilation strategies satisfies the ASHRAE standard 55 recommendation of PMV range (from -0.5 to 0.5) for all occupants throughout the response period while the supply air temperature is 4 C higher under displacement ventilation. Moreover, as the internal heat load increases, PMVs decrease more rapidly for displacement ventilation than mixing ventilation.

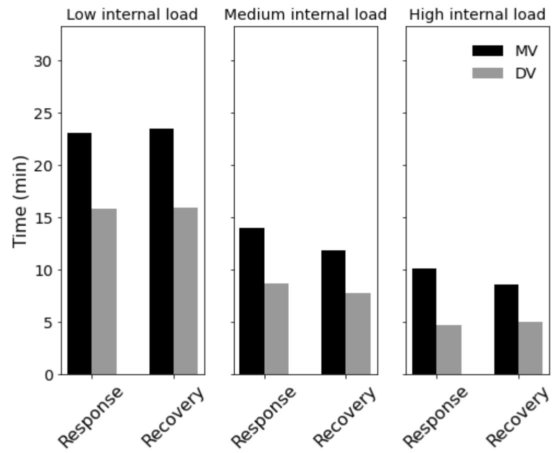

Figure 7 One time constant of air temperature in ASHRAE breathing zone for low, medium, and high internal loads.

During the first 30 minutes are steady-state region before the response period, for low internal load, the steady-state PMVs range from -0.34 to -0.32 for displacement ventilation and -0.42 to -0.14 for mixing ventilation. For high internal load, it ranged from -1.25 to -0.76 for displacement ventilation and -0.85 to -0.41 for mixing ventilation. When comparing the low and high internal loads for each ventilation strategy, the average difference in steady-state PMV occurring before the response period is 0.38 for the eight occupants under mixing ventilation, while it is 0.71 for displacement ventilation. This result implies a greater opportunity for displacement ventilation to increase the magnitude of a global temperature adjustment, thus reducing even more energy used for cooling. This phenomenon can be attributed to the distribution of load within space. Under displacement ventilation, the lighting load on the ceiling has less impact on occupants' thermal sensation compared to mixing ventilation, due to stratification.

Another aspect to consider is the spatial variation of the PMV among occupants. Under displacement ventilation at a low internal load, the PMV was almost uniform across all occupants. In contrast, those under mixing ventilation experienced variations in PMV from one area to another. As the internal heat load increases, the PMV shows significant variation within the space for both ventilation strategies, especially under displacement ventilation. Increased internal loads from low to high, each accompanied by a corresponding higher supply air flow rate, has led occupants to experience varied PMV across different areas. The standard deviations of the average PMV before the response period were 0.01 for low and 0.13 for high internal loads, respectively. This suggests that thermal comfort uniformity is achieved by reducing the supply air flow rate and velocity.

Unsteady PMVs

Figures 8 and 9 also illustrate the unsteady-state conditions, denoted as τ, which correspond to response and recovery phases over one time constant of an ASHRAE breathing zone temperature increase. During the temperature ramp up in an ASHRAE breathing zone, PMV increases as well. However, under conditions of low internal load, the augmentation in PMV values, quantified over a single time constant, was found to be markedly elevated for the same occupants under displacement ventilation. Specifically, this increase ranged from 13% to 29% as opposed to the corresponding values observed under mixing ventilation. With less time required to reach the one time constant observed under displacement ventilation, it is salient to note that occupants, under conditions of low internal thermal load, manifest a more accelerated and pronounced alteration in thermal comfort.

(a) Displacement – Low internal load

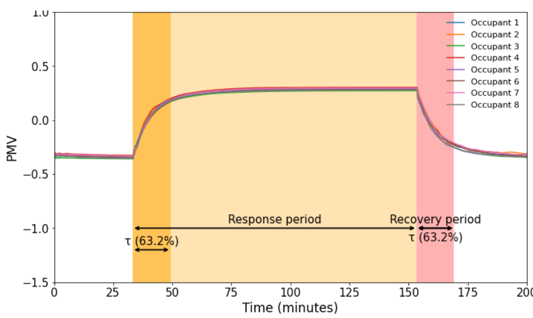

(b) Mixing – Low internal load

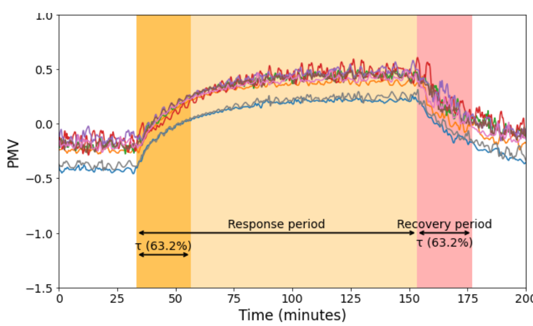

Figure 8 Predicted mean vote (PMV) of the eight occupants. (a) displacement and (b) mixing ventilation at low internal load. The light orange, thick orange, and red region indicating response period, one time constant of the ASHRAE breathing zone temperature during response and recovery period, respectively.

Draft risk

Figures 10 and 11 illustrate the dynamics of draft risks at ankle and head levels for low and high internal loads, incorporating mixing and displacement ventilation strategies. Draft risk tends to reduce during the response period due to the elevated supply air temperature. In a steady-state condition, draft risk fluctuates within a wider range for mixing ventilation than displacement ventilation. However, displacement ventilation exhibits a greater fluctuation of draft risk in an unsteady-state condition, suggesting heightened susceptibility to changes in supply air temperature. This can likely be ascribed to perturbations in the stratification of temperature, precipitated by the direct supply of warmer air at floor level. Figure 12 (a) elucidates that for displacement ventilation under low internal load, there is a notable decrease in vertical temperature difference at the commencement of the response period, followed by an increase at the outset of the recovery period. In the context of mixing ventilation, the vertical temperature differential remains comparatively stable within its operating range, although this range does expand with increasing internal load. Moreover, the spatial distribution of draft risk is accentuated under displacement ventilation, particularly under high internal load conditions.

As substantiated by Figure 11 (a) and (c), the spatial variability in ankle draft risk is more expansive in environments utilizing displacement ventilation. Conversely, in mixing ventilation setups, there is increased volatility and generally elevated draft risk levels at both ankle and head heights, irrespective of occupant location.

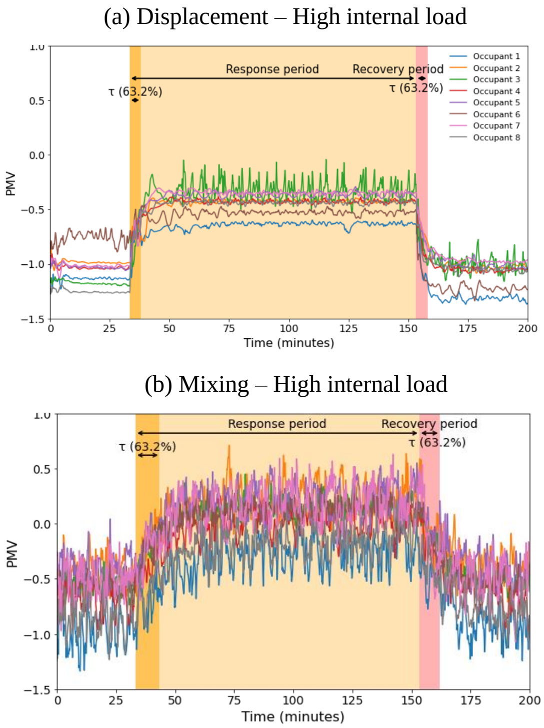

Figure 9 Predicted mean vote (PMV) of the eight occupants. (a) displacement and (b) mixing ventilation at low internal load.

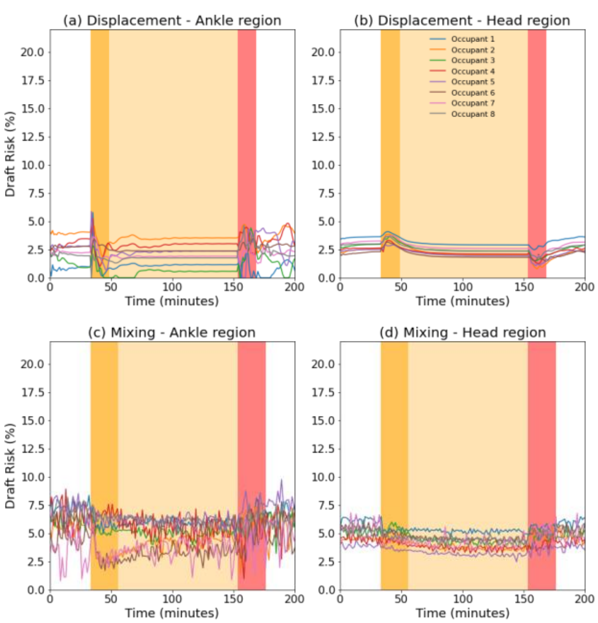

Figure 10 Draft risks of eight occupants at Low internal across different sampling regions. a) displacement – ankle (b) displacement – head (c) mixing – ankle (d) mixing – head.

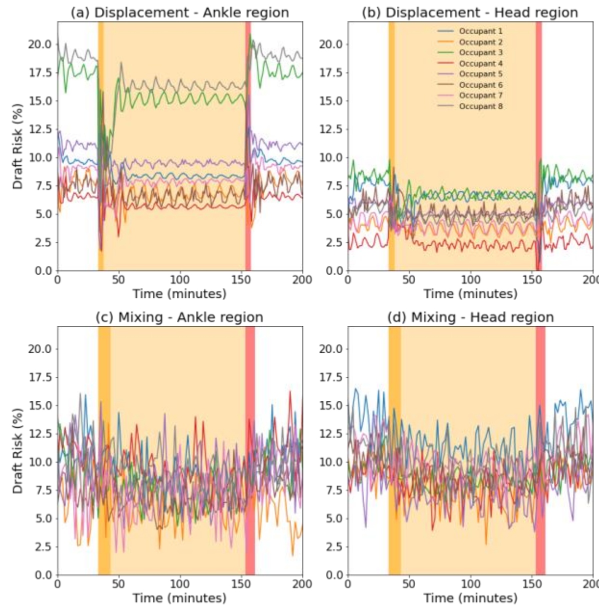

Figure 11 Draft risks of eight occupants under mixing and displacement ventilation at High internal across different sampling regions. a) displacement – ankle (b) displacement – head (c) mixing – ankle (d) mixing – head.

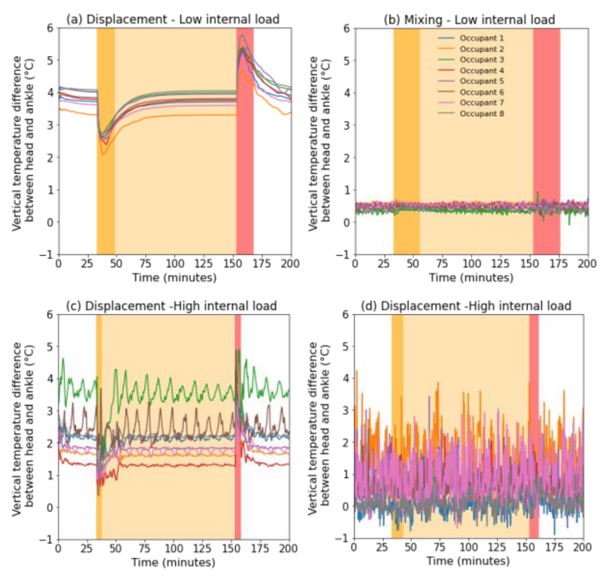

Figure 12 Vertical temperature difference between head and ankle at Low and High internal load under mixing and displacement ventilation

Conclusion

This study evaluated occupants' thermal comfort during a global temperature adjustment based on steady- and unsteady-state PMVs, draft risk, and local thermal comfort at ankle, chest, and head levels. Based on CFD simulations, unsteady-state PMVs were estimated until the one-time constant after a temperature change whereas steady-state PMVs were estimated from the one time constant to the end of a response or recovery period. The evaluations were performed for two distinct ventilation systems—mixing and displacement ventilation—across three internal load intensities. The results are as follow:

1) The study found that ASHRAE breathing zone temperatures respond 31% to 54% faster under displacement ventilation compared to mixing ventilation. The difference becomes more pronounced with increasing internal loads.

2) As the type of internal load transitions from low to high, initial steady-state average PMV decreases by 0.71 and 0.38 under displacement and mixing ventilation, respectively, suggesting greater opportunities for global temperature adjustment strategies to save cooling energy further.

3) The change rate of PMVs during unsteady-state is 13-29% higher for displacement ventilation than mixing ventilation, especially under low internal loads, indicating faster and higher alterations in thermal comfort among occupants.

4) Draft risk profiles exhibited distinct characteristics under the two ventilation strategies. Mixing ventilation displayed a wider band of fluctuations in a steady-state environment, while displacement ventilation exhibited more pronounced fluctuations under unsteady-state conditions, particularly at high internal loads.

Acknowledgment

This work was supported by the new faculty research fund of Ajou University.

References

Albadi MH, El-Saadany EF. A summary of demand response in electricity markets. Electric Power Systems Research 2008;78:1989–96, doi:10.1016/j.epsr.2008.04.002.

Aghniaey S, Lawrence TM. The impact of increased cooling setpoint temperature during demand response events on occupant thermal comfort in commercial buildings: A review. Energy and Buildings 2018;173:19–27, doi:10.1016/j.enbuild.2018.04.068.

Ahn H, Rim D, Lo LJ. Ventilation and energy performance of partitioned indoor spaces under mixing and displacement ventilation. Build Simul 2018;11:561–74. doi:10.1007/s12273-017-0410-z.

Albadi MH, El-Saadany EF. Demand Response in Electricity Markets: An Overview. 2007 IEEE Power Engineering Society General Meeting, 2007, p. 1–5. https://doi.org/10.1109/PES.2007.385728.

Arens E, Zhang H, Huizega C. Partial- and whole-body thermal sensation and comfort – Part 1: Uniform environmental conditions. Journal of Thermal Biology 2006;31:53-59, https://doi.org/10.1016/j.jtherbio.2005.11.028.

ASHRAE. ASHRAE Standard 55: Thermal environmental conditions for human occupancy. American Society of Heating, Refrigerating and Air-Conditioning Engineers, 2020, Atlanta.

Cui B, Gao D, Wang S, Xue X. Effectiveness and life-cycle cost-benefit analysis of active cold storages for building demand management for smart grid applications. Applied Energy 2015;147:523–35, doi:10.1016/j.apenergy.2015.03.041.

D. N. Sørensen and L. K. Voigt, “Modelling flow and heat transfer around a seated human body by computational fluid dynamics,” Build Environ, vol. 38, no. 6, pp. 753–762, 2003, doi: 10.1016/S0360-1323(03)00027-1.

González-Torres M, Pérez-Lombard L, Coronel JF, Maestre IR, Yan D. A review on buildings energy information: Trends, end-uses, fuels and drivers. Energy Reports 2022;8:626–37, doi:10.1016/j.egyr.2021.11.280.

Hamm R, Whitlock D, Eatinger R, Stearns J, Ringwood S. Implementation of a Temperature Ramp Rate Requirement and Impact on the Packaging Processes. International Symposium on Microelectronics 2018;2018:000494–507, doi:10.4071/2380-4505-2018.1.000494.

Hu M, Xiao F, Jørgensen JB, Wang S. Frequency control of air conditioners in response to real-time dynamic electricity prices in smart grids. Applied Energy 2019;242:92–106. doi:10.1016/j.apenergy.2019.03.127.

I. B. Celik, U. Ghia, P. J. Roache, C. J. Freitas, H. Coleman, and P. E. Raad, “Procedure for estimation and reporting of uncertainty due to discretization in CFD applications,” Journal of Fluids Engineering, Transactions of the ASME, vol. 130, no. 7, pp. 0780011–0780014, Jul. 2008, doi: 10.1115/1.2960953.

Korkas CD, Baldi S, Michailidis I, Kosmatopoulos EB. Occupancy-based demand response and thermal comfort optimization in microgrids with renewable energy sources and energy storage. Applied Energy

2016;163:93–104, doi:10.1016/j.apenergy.2015.10.140.

Li X, Malkawi A. Multi-objective optimization for thermal mass model predictive control in small and medium size commercial buildings under summer weather conditions. Energy 2016;112:1194–206, doi:10.1016/j.energy.2016.07.021.

Li X, Wen J, Malkawi A. An operation optimization and decision framework for a building cluster with distributed energy systems. Applied Energy 2016;178:98–109. https://doi.org/10.1016/j.apenergy.2016.06.030.

Li Z, Meng Q, Wei Y, Zhang L, Sun Z, Lei Y, et al. Dynamic room temperature setpoints of air-conditioning demand response based on heat balance equations with thermal comfort model as constraint: On-site experiment and simulation. Journal of Building Engineering 2023;65:105798. https://doi.org/10.1016/j.jobe.2022.105798.

Luo Z, Peng J, Cao J, Yin R, Zou B, Tan Y, et al. Demand Flexibility of Residential Buildings: Definitions, Flexible Loads, and Quantification Methods. Engineering 2022;16:123–40. https://doi.org/10.1016/j.eng.2022.01.010.

Motegi N, Piette MA, Watson DS, Kiliccote S, Xu P. Introduction to Commercial Building Control Strategies and Techniques for Demand Response -- Appendices. 2007. https://doi.org/10.2172/1004169.

Ning B, Schiavon S, Bauman FS. A Classification Scheme for Radiant Systems based on Thermal TimeConstant 2015.

P. O. Fanger, A. K. Melikov, H. Hanzawa, and J. Ring, “Air Turbulence and Sensation of Draught,” 1988.

Pallonetto F, De Rosa M, Finn DP. Impact of intelligent control algorithms on demand response flexibility and thermal comfort in a smart grid ready residential building. Smart Energy 2021;2:100017. https://doi.org/10.1016/j.segy.2021.100017.

Pedersen TH, Hedegaard RE, Kristensen KF, Gadgaard B, Petersen S. The effect of including hydronic radiator dynamics in model predictive control of space heating. Energy and Buildings 2019;183:772–84. https://doi.org/10.1016/j.enbuild.2018.11.015.

Romero Rodríguez L, Brennenstuhl M, Yadack M, Boch P, Eicker U. Heuristic optimization of clusters of heat pumps: A simulation and case study of residential frequency reserve. Applied Energy 2019;233–234:943–58. https://doi.org/10.1016/j.apenergy.2018.09.103.

Romero Rodríguez L, Sánchez Ramos J, Álvarez Domínguez S, Eicker U. Contributions of heat pumps to demand response: A case study of a plus-energy dwelling. Applied Energy 2018;214:191–204. https://doi.org/10.1016/j.apenergy.2018.01.086.

Shan K, Wang S, Yan C, Xiao F. Building demand response and control methods for smart grids: A review. Science and Technology for the Built Environment 2016;22:692–704. https://doi.org/10.1080/23744731.2016.1192878.

Wang H, Wang S, Tang R. Development of grid-responsive buildings: Opportunities, challenges, capabilities and applications of HVAC systems in non-residential buildings in providing ancillary services by fast demand responses to smart grids. Applied Energy 2019;250:697–712. https://doi.org/10.1016/j.apenergy.2019.04.159.

Wu Q, Liu J, Zhang L, Zhang J, Jiang L. Study on thermal sensation and thermal comfort in environment with moderate temperature ramps. Building and Environment 2020;171:106640. https://doi.org/10.1016/j.buildenv.2019.106640.

Wu X, Liu Y, Liu G, Wang F, Wang Z. Effect of Supply Air Temperature on Indoor Thermal Comfort in a Room with Radiant Heating and Mechanical Ventilation. Energy Procedia 2017;121:206–13. https://doi.org/10.1016/j.egypro.2017.08.019.

X. Shan, J. Zhou, V. W. C. Chang, and E. H. Yang, “Comparing mixing and displacement ventilation in tutorial rooms: Students’ thermal comfort, sick building syndromes, and short-term performance,” Build Environ, vol. 102, pp. 128–137, Jun. 2016, doi: 10.1016/j.buildenv.2016.03.025.

Y. Cheng, Z. Lin, and A. M. L. Fong, “Effects of temperature and supply airflow rate on thermal comfort in a stratum-ventilated room,” Build Environ, vol. 92, pp. 269–277, Sep. 2015, doi: 10.1016/j.buildenv.2015.04.036.

Yang X, Chen Z, Huang X, Li R, Xu S, Yang C. Robust capacity optimization methods for integrated energy systems considering demand response and thermal comfort. Energy 2021;221:119727. https://doi.org/10.1016/j.energy.2020.119727.

Yin R, Ghatikar G, Piette M. Big-Data Analytics for Electric Grid and Demand-Side Management. 2019. https://doi.org/10.2172/1773709.

Yin R, Kara EC, Li Y, DeForest N, Wang K, Yong T, et al. Quantifying flexibility of commercial and residential loads for demand response using setpoint changes. Applied Energy 2016;177:149–64. https://doi.org/10.1016/j.apenergy.2016.05.090.

Yoon JH, Baldick R, Novoselac A. Demand response control of residential HVAC loads based on dynamic electricity prices and economic analysis. Science and Technology for the Built Environment 2016;22:705–19. https://doi.org/10.1080/23744731.2016.1195659.